METEOROLOGICAL APPLICATIONS
Meteorol. Appl. (2010)
Published online in Wiley InterScience
(www.interscience.wiley.com) DOI: 10.1002/met.176

RMetS
Royal Meteorological Society

Application of Meteosat second generation data towards improving the nowcasting of convective initiation

Christopher W. Siewert,[a]* Marianne Koenig[a] and John R. Mecikalski[b]
[a] *EUMETSAT, Darmstadt, 64295, Germany*
[b] *Atmospheric Science Department, University of Alabama in Huntsville, Huntsville, AL, USA*

ABSTRACT: The prediction of convective initiation (CI) from a satellite perspective provides forecasters with a constant relatively high temporal and convective scale spatial resolution tool to help protect life and property. By monitoring infrared (IR) channel brightness temperatures, their trends and multi-spectral channel differences, the prediction of CI can be accomplished on the 0–1 h timescale. These methods, currently employed on the Geostationary Operational Environmental Satellite (GOES) system, have only recently been explored on the Meteosat Second Generation (MSG) satellite system. The additional channels and derived instability indices available on the MSG satellites may provide additional information useful to the prediction of CI. In this paper a concept is developed and discussed towards the advantages and possible applications of the inclusion of MSG specific IR spectral channels and instability information through the analysis of several convective case events over Central Europe and South Africa. Copyright © 2010 Royal Meteorological Society

KEY WORDS satellite; nowcasting; convection

Received 27 April 2009; Revised 28 October 2009; Accepted 3 November 2009

1. Introduction

The use of satellites to predict convection has been ongoing for over 40 years (Riehl and Schleusener, 1962; Purdom, 1976; Adler and Fenn, 1979; Purdom, 1982; Setvak and Doswell, 1991; Strabala *et al*., 1994; Roberts and Rutledge, 2003; Setvak *et al*., 2003; Mecikalski and Bedka, 2006; Mecikalski *et al*., 2008; Mackenzie *et al*., 2010). The use of geostationary satellite imagery, in particular in the study of convection, provides multiple advantages. Geostationary satellite data allows for a constant view of the same area with relatively high temporal and convective scale spatial resolution. Providing forecasters with satellite data to predict convective initiation (CI), or the first occurrence of a 35 dBZ radar echo at ground level, has been shown to increase significantly the detection CI *versus* the use of radar alone in National Weather Service offices throughout the United States (Roberts and Rutledge, 2003). With infrared (IR) channel spatial resolutions up to 3 km^2 at nadir and scan times from 5 to 15 min for the Meteosat Second Generation (MSG) satellites (Schmetz *et al*., 2002), the CI process is well observed at scales from meso-γ to meso-β (2–200 km).

Previous efforts have shown that the CI process can be forecast up to 1 h prior to its occurrence through the use of IR satellite data alone (Roberts and Rutledge, 2003; Mecikalski and Bedka, 2006). The framework described in Mecikalski and Bedka (2006) includes the use of eight 'interest fields' to forecast the occurrence of CI within the 0–1 h timeframe based on IR channel brightness temperatures, trends and multi-spectral channel differences. These interest fields were developed for use on the Geostationary Operational Environmental Satellite (GOES) system, particularly GOES-12, which provides coverage over the eastern half of the United States. Currently, techniques based on the Mecikalski and Bedka (2006) framework are employed by multiple agencies to detect threats to public safety and aviation in real-time situations (Mecikalski *et al*., 2007).

Recent studies have found that the additional channels on the MSG satellites may provide additional information useful to the prediction of CI over the 0–1 h time frame (Mecikalski *et al*., 2010). Analyzing the benefits of increased spectral and spatial resolution and employing the techniques described in Mecikalski and Bedka (2006) on the MSG system will be useful in both increasing the ability of forecasters to predict potentially hazardous weather conditions associated with thunderstorms, as well as providing insight into the increased capabilities of the next generation of GOES satellites, whose spectral channels will be similar to those already established on the MSG satellites (Schmetz *et al*., 2002; Schmit *et al*., 2005).

In this paper a concept is developed and discussed towards the advantages and possible applications of the inclusion of MSG specific interest fields and derived instability indices through the analysis of convective case events over Central Europe and South Africa. Section 2 discusses the data and methods used to analyze the

* Correspondence to: Christopher W. Siewert, EUMETSAT, Darmstadt, Germany. E-mail: chris.siewert@noaa.gov

Copyright © 2010 Royal Meteorological Society

case events presented and described in detail in Section 3. Section 4 presents a brief discussion of the results of the study and Section 5 presents the conclusions drawn from the results and suggests future work to further the understanding of the improvements of CI nowcasting.

2. Data and methodology

2.1. MSG satellite

The Spinning Enhanced Visible and Infrared Imager (SEVIRI) on board the MSG-2 (Meteosat-9) satellite contains 12 spectral channels: 3 visible, 1 near-IR and 8 IR, shown in Table I (Schmetz *et al*., 2002). Imagery data were provided in-house at the EUMETSAT facilities located in Darmstadt, Germany. In comparison, the imager on board the GOES-12 satellite contains only one visible and four IR channels, centred at 0.65, 3.9, 6.5, 10.7, and 13.3 μm respectively. The additional channels available on the MSG-2 satellite provide a wider range of spectral information including microphysical information from the 1.6 μm (Setvak *et al*., 2003; Rosenfeld *et al*., 2008) and 8.7 μm channels (Strabala *et al*., 1994), as well as water vapour and ozone measurements from the 7.3 and 9.7 μm channels respectively. Also, the 12.0 and 13.4 μm channels on SEVIRI allow for an improved assessment of cloud depth and microphysics (Prata, 1989). The recent work by Mecikalski *et al*. (2010) shows several new insights towards the nowcasting of CI with SEVIRI, in addition to the current information retrieved from the channels available on the GOES-12 satellite (Setvak and Doswell, 1991; Ackerman, 1996; Schmetz *et al*., 1997; Roberts and Rutledge, 2003; Mecikalski and Bedka, 2006; Mackenzie *et al*., 2010).

Table I. List of channels available on SEVIRI from Schmetz *et al*. (2002).

Channel no.		Characteristics of spectral band (μm)			Main gaseous absorber or window
		λ_{cen}	λ_{min}	λ_{max}	
1	VIS0.6	0.635	0.56	0.71	Window
2	VIS0.8	0.81	0.74	0.88	Window
3	NIR1.6	1.64	1.50	1.78	Window
4	IR3.9	3.90	3.48	4.36	Window
5	WV6.2	6.25	5.35	7.15	Water vapour
6	WV7.3	7.35	6.85	7.85	Water vapour
7	IR8.7	8.70	8.30	9.10	Window
8	IR9.7	9.66	9.38	9.94	Ozone
9	IR 10.8	10.80	9.80	11.80	Window
10	IR 12.0	12.00	11.00	13.00	Window
11	IR 13.4	13.40	12.40	14.40	Carbon dioxide
12	HRV	Broadband (about 0.4–1.1)			Window/water vapour

2.2. CI nowcasting techniques

The occurrence of a 35 dBZ radar echo within a growing cumulus cloud suggests a strong correlation with continual development into the mature cumulus stage and precipitation at the ground (Roberts and Rutledge, 2003). The goal of CI nowcasting is to provide insight into which cumulus clouds (out of the typically large population of these clouds present on a given day) will begin to precipitate with echo intensity $\geq$35 dBZ, and possibly develop in to thunderstorms in the 0–1 h timeframe. Early methods of CI nowcasting were developed using 10.8 μm brightness temperature measurements and monitoring their 15 and 30 min trends to determine cloud-top heights and growth rates (Roberts and Rutledge, 2003). Multi-spectral channel differences such as the 6.5–10.8 μm (Ackerman, 1996; Schmetz *et al*., 1997) and 13.3–10.8 μm (Ellrod, 2004; Mecikalski and Bedka, 2006) channel differences and their trends were also found to be useful in identifying and diagnosing cloud-top height, width and growth. In combination, Mecikalski and Bedka (2006) developed eight CI interest fields from GOES which would be used in conjunction to identify immature cumulus clouds that would eventually grow into mature precipitating cumulus clouds within the 0–1 h time-frame. Mecikalski and Bedka (2006) make their CI 'nowcasts' based on a simple scoring technique, where seven of the eight interest fields must meet their individual threshold values for an individual pixel to be labelled a 'threat' for CI. These interest fields, shown in Table II, present a variety of physical processes occurring within the immature cumulus cloud associated with convective growth (see Mecikalski and Bedka, 2006). Using various combinations of the interest fields have shown that this method provides probability of detection (POD) values maximizing around 99%, while false alarm rates (FAR) minimize near 69% (Mecikalski *et al*., 2008). It is now recognized that one way to minimize FARs is to either constrain the satellite estimates of CI prediction with numerical weather prediction- or satellite-based fields (e.g. convective available potential energy, convective inhibition), and/or to treat clusters of pixels of cumulus clouds as single cumulus 'objects'. Both of these ideas are subjects of ongoing research (see NOAA NESDIS ATBD; Mecikalski *et al*., 2008).

Mecikalski *et al*. (2010) found that by using IR data alone the MSG channels provide up to 67 possible CI interest fields. Upon completion of a detailed correlation and principal component analyses, less than half were found to be unique indicators (i.e. containing non-redundant information) during the CI process as observed during the Convective and Orographically-induced Precipitation Study (COPS) field study of 2007 over southern Germany and northeastern France (Wulfmeyer *et al*., 2008; www.cops2007.de). One set of IR fields from MSG that contain unique information, their mean values and standard deviations, is shown in Table III. These interest fields have been grouped into three categories by Mecikalski *et al*. (2010) based on their ability to describe

Copyright © 2010 Royal Meteorological Society

DOI: 10.1002/met

Table II. List of the Mecikalski and Bedka (2006) CI indicators, their physical basis and critical threshold values.

CI interest field	Purpose and resolution	MB06 critical value
6.5–10.7 μm difference	4 km cloud-top height relative to upper-tropospheric WV weighting function (Schmetz *et al*., 1997)	−35 to −10 °C
13.3–10.7 μm difference	8 km cloud-top height assessment/updraft width	−25 to −5 °C
10.7 μm T_B	4 km cloud-top glaciation (Roberts and Rutledge, 2003)	$-20 < T_B < 0$ °C
10.7 μm T_B drop below 0 °C	4 km cloud-top glaciation (Roberts and Rutledge, 2003)	Within prior 30 min
10.7 μm T_B time trend (15 and 30 min)	4 km cloud-top growth rate/updraft strength (Roberts and Rutledge, 2003)	<-4 °C (15 min)$^{-1}$ ΔT_B (30 min)$^{-1}$ $< \Delta T_B$ (15 min)$^{-1}$
6.5–10.7 μm time trend	4 km multispectral cloud growth	>3 °C (15 min)$^{-1}$
13.3–10.7 μm time trend	8 km multispectral cloud growth	>3 °C (15 min)$^{-1}$

the physical processes they represent as important to the CI process: cloud depth, cloud-top glaciation and updraft strength. For this study the top 4 interest fields from 'cloud depth' and 'cloud-top glaciation', and the top 5 from 'updraft strength' were combined with the existing 8 CI interest fields developed by Mecikalski and Bedka (2006). Only the top 4 or 5 were used in order to minimize the amount of redundancy within the interest fields' representative physical processes.

In the event where an MSG interest field was similar to that from the original Mecikalski and Bedka (2006) study, the threshold values for those interest fields were left at the original critical values. Confidence in doing this was high given that the GOES channels used in the Mecikalski and Bedka (2006) study are very similar to these MSG channels, in terms of spectral width, and central wavenumber (Schmetz *et al*., 2002; Schmit *et al*., 2005). However, in order to determine appropriate threshold values for the new interest fields, adjustments were made to the mean values by adjusting the threshold value up to one standard deviation away from the mean value such that the largest population of events would be included and still remain physically explainable. For example, the 12.0–10.8 μm channel difference with a mean value of −1.08 °C and a standard deviation of 1.15 °C was adjusted to have a threshold value of 0 °C, since a positive value in this channel difference would retain no physical basis towards CI (Mecikalski and Bedka, 2006, and references therein).

In addition to the new interest fields provided by the results from the Mecikalski *et al*. (2010) study, MSG-specific operationally produced Global Instability Index (GII) Lifted Index and K-Index (see Koenig and de Coning, 2009) convective instability fields were used to identify regions conducive to future convective development given that sufficient instability exists to support thunderstorms. With the addition of pre-convective state information, an assessment of the potential 'strength' of each CI nowcast may be accomplished. This is a unique aspect of the present study compared to previous research. In total, 19 CI interest fields were used here, which are presented along with their physical representation in Table IV. For this study it is a requirement that 16 of the 19 interest fields must be met for an individual pixel to be labelled

Table III. List of additional MSG specific interest fields, their mean values and standard deviations from Mecikalski *et al*. (2009a).

Cloud depth	Mean	Standard deviation
6.2–10.8 μm difference	−22.05°	11.27°
10.8 μm T_B	252.02 K	16.79°
6.2–7.3 μm difference	−9.52°	5.94°
12.0–10.8 μm difference	−1.08°	1.15°
0.6 μm reflectance (for optical depth)	0.305	0.173
0.8 μm reflectance (for optical depth)	0.360	0.188
30 min trend 0.6 μm reflectance	0.024	0.087
30 min trend 0.8 μm reflectance	0.021	0.087
Cloud-top glaciation	**Mean**	**Standard deviation**
(8.7–10.8 μm)–(10.8–12.0) 'Tri-channel'	−1.29°	1.94°
30 min trend tri-channel	1.59°	1.96°
8.7–10.8 μm difference	−0.21°	1.55°
15 min trend tri-channel	0.87°	2.02°
3.9–10.8 μm difference	−0.79°	0.41°
15 min trend 3.9–10.8 μm difference	0.30°	0.24°
1.6 μm reflectance	0.173	0.091
30 min trend 1.6 μm reflectance	−0.040	0.069
3.9 μm reflectance	0.050	0.038
Updraft strength	**Mean**	**Standard deviation**
30 min 10.8 μm T_B trend	−18.04°	13.54°
30 min trend 12.0–10.8 μm difference	0.26°	1.17°
15 min trend 12.0–10.8 μm difference	0.18°	1.05°
15 min 10.8 μm T_B trend	−11.14°	9.44°
30 min trend 8.7–10.8 μm difference	1.33°	1.54°
HRV cloud texture	n/a	n/a

Copyright © 2010 Royal Meteorological Society

DOI: 10.1002/met

Table IV. List of the 19 CI interest fields used in this study, their physical basis and critical threshold values.

Interest field	Physical basis (Mecikalski *et al.*, 2009a)	Critical value
10.8 μm T_B	Cloud-top height/glaciation	−20-0 °C
10.8 μm T_B drop below 0 °C	Cloud-top glaciation	Within prior 30 min
10.8 μm 15 min trend	Cloud growth rate	<−4 °C
10.8 μm 30 min trend	Cloud growth rate	<15 min trend
6.2–7.3 μm difference	Breaking of capping inversion/cloud depth	−25-3 °C
6.2–10.8 μm difference	Cloud height relative to dry air aloft	−35-−10 °C
6.2–10.8 μm 15 min trend	Cloud growth towards dry air aloft	>3 °C
8.7–10.8 μm difference	Cloud-top glaciation	−10-0 °C
8.7–10.8 μm 30 min trend	Cloud-top glaciation growth	0–10 °C
12.0–10.8 μm difference	Height relative to mid- to upper-troposphere	−3-0 °C
12.0–10.8 μm 15 min trend	Cloud growth toward mid- to upper-troposphere	>0 °C
12.0–10.8 μm 30 min trend	Cloud growth toward mid- to upper-troposphere	>0 °C
13.4–10.8 μm difference	Cloud height/updraft volume	−25-−5 °C
13.4–10.8 μm 15 min trend	Cloud height/updraft volume growth	>3 °C
Tri-channel difference [(8.7–10.8)–(10.8–12.0)]	Cloud-top glaciation	−10-0 °C
Tri-channel 15 min trend	Cloud-top glaciation growth	>0 °C
Tri-channel 30 min trend	Cloud-top glaciation growth	>0 °C
GII K-index	Convective potential	>25
GII lifted index	Convective potential	<−2

as a threat for CI, with any pixels meeting 18 or more fields labelled as strong indicators of CI.

2.3. Cloud identification and tracking

In order to identify cloud pixels within a scene, a (convective) cloud masking technique is necessary to both reduce processing time such that real-time CI nowcasts may be made feasibly, as well as help reduce false-alarm nowcasts. To accomplish this, a simple 'yes or no' cloud mask provided operationally by EUMETSAT (Lutz, 2007) was used to determine which pixels were to be included into the CI nowcasting algorithm. This method, although not as sophisticated as those based on cluster analysis techniques (Nair *et al.*, 1998; Berendes *et al.*, 2008), is readily available to any user of MSG data and provided in the time periods necessary for real-time nowcasting purposes.

Once a cloud pixel is identified it must be followed through 15 and 30 min in which the individual brightness temperature and multi-spectral channel difference trends are to be calculated. The simplest and most computationally inexpensive method available to accomplish this is known as the 'box-averaging' method developed by the University of Wisconsin's Cooperative Institute for Meteorological Satellite Studies (see NOAA NESDIS ATBD; Mecikalski *et al.*, 2008). In essence, a box of cloud pixels is expanded around a single cloudy pixel and that pixel's individual channel average brightness temperature is based solely on the temperature of the cloudy pixels around it within the box, assumed to be representative of that individual cumulus cloud. In this study, a 7×7 pixel box was used to represent the area in which a single cloud pixel is expected to move over a 30 min time period. At nadir this sized box represents a cloud motion of about 42 km h^{-1}. As the distance from nadir increases however, the box's representative cloud motion will also increase. Also, in order to increase the accuracy of the box-averaging cloud tracking technique, multiple 'risk reduction' measures are used to eliminate regions affected by expanding cloud edges and cirrus contamination (NOAA NESDIS ATBD; Mecikalski *et al.*, 2008).

3. Results

Two events during the year 2008 where significant CI took place will be used for discussion in this study. The first, a severe weather event which included reports of tornado damage and large hail by the European Severe Storms Laboratory's European Severe Weather Database, occurred over Eastern Germany and the Czech Republic on 31 May 2008. This event will be discussed in detail regarding the individual MSG specific interest fields and the role they played in affecting the CI nowcasts. The other case, representing a typical CI event over the southern half of Africa during the Southern Hemisphere summer, took place over the eastern half of South Africa during the month of February 2008 and will be discussed briefly as a comparison. Each event will be reviewed regarding the periods prior to and during CI based on the nowcasts produced by both the Mecikalski and Bedka (2006) method and the method described above for MSG.

3.1. 31 May 2008

Beginning at about 1100 UTC on 31 May 2008, convection began forming in an area of strong convergence and orographic lifting along the northern border of the Czech Republic. These convective cells would eventually be linked to reports of heavy rain, large hail, funnel clouds and possible tornado damage in the Czech Republic and eastern Germany in the following hours. These

Copyright © 2010 Royal Meteorological Society

DOI: 10.1002/met

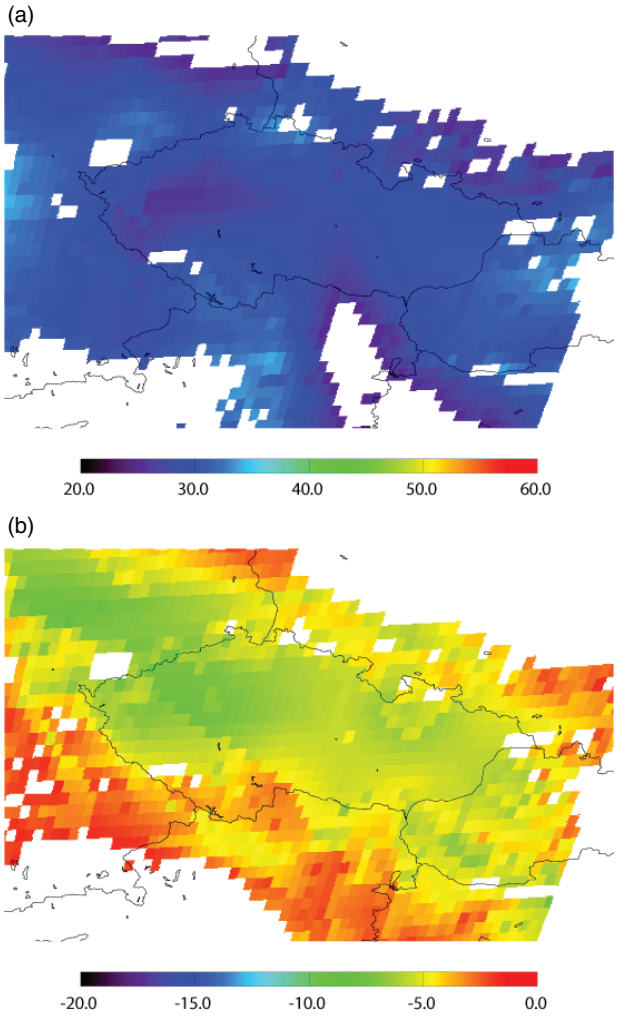

Figure 1. Images of 31 May 2008 nowcast time period 1100 UTC Global Instability Index (GII) derived (a) K-Index and (b) Lifted Index values.

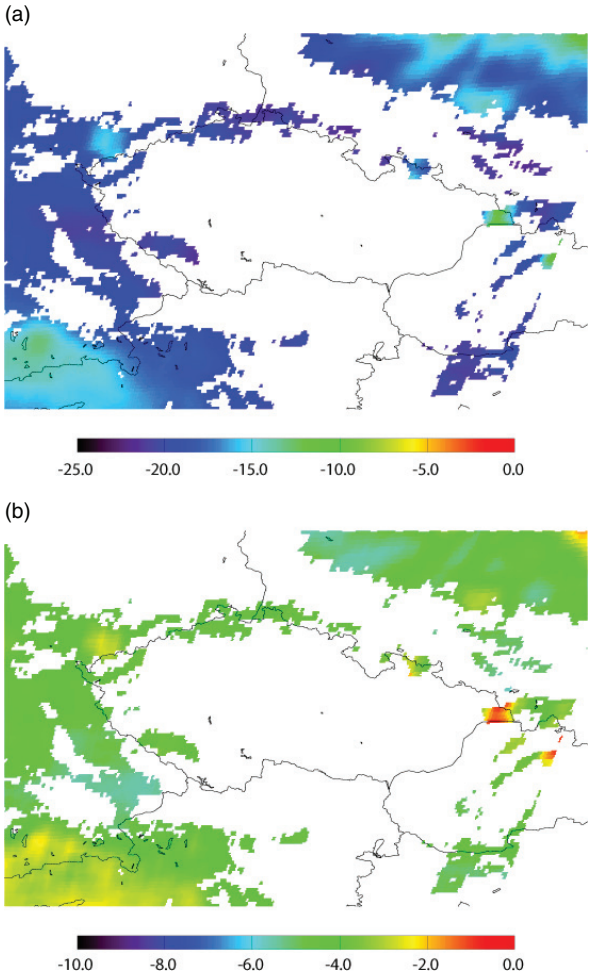

Figure 2. Images of 31 May 2008 nowcast time period 1100 UTC (a) 6.2–7.3 μm channel difference and (b) tri-channel [(8.7–10.8)–(10.8–12.0)] μm difference.

storms formed very rapidly due to the complex terrain and relatively high instability in the area (Figure 1(a) and (b). Figure 1(a) shows the GII derived K-Index values over the region for 1100 UTC. K-Index values reaching near 35 were seen, which is fairly significant for central Europe. Similarly, Figure 1(b) shows Lifted Index reaching -10° over the same area, suggesting that the potential for severe convection is significantly increased. These fields, which are available operationally to users of MSG data, when included into the MSG CI nowcast provided useful support for an experimental CI strength indicator that will be discussed further in the coming sections.

Figure 2(a) and (b) shows examples of the new MSG specific 6.2–7.3 μm and tri-channel difference interest fields developed by Mecikalski *et al.* (2010). The 6.2–7.3 μm channel difference, shown in Figure 2(a), reaches threshold values along the northern border of the Czech Republic at this time period. With values exceeding −10 K, the 6.2–7.3 μm channel difference is showing convective cloud tops near to breaking the capping inversion and promoting further development (Mecikalski *et al.*, 2010). Similarly, the [(8.7–10.8 μm)–(10.8–12.0 μm)] difference, shown in Figure 2(b), reaches values very near 0 K, which suggests strong cloud top glaciation (Mecikalski *et al.*, 2010).

Figure 3(a) and (b) shows the 8.7–10.8 μm channel difference and 30-min trend for the same time period over the Czech Republic. Similar to the tri-channel difference, the 8.7–10.8 μm channel difference is showing strong signs of cloud top glaciation along the northern Czech Republic border, with values nearing 0 K (Figure 3(a)). The 30 min trend in the 8.7–10.8 μm channel difference, representing cloud-top glaciation growth rate (Mecikalski *et al.*, 2010), also shows a signal in the same area with values exceeding 2 K over 30 min. Figure 4(a) and (b) also shows these signals using the tri-channel 15 and 30 min trends. Similar to the 8.7–10.8 μm channel difference trends, the tri-channel difference trends represent growth in cloud-top glaciation, and thus identifying regions where significant updrafts are persistent (Mecikalski *et al.*, 2010).

Figure 5(a) and (b) shows the two versions of the CI nowcast produced during this time period overlaid on 10.8 μm brightness temperatures, with CI nowcasts presented in red. This process of overlaying the nowcasts

Copyright © 2010 Royal Meteorological Society

DOI: 10.1002/met

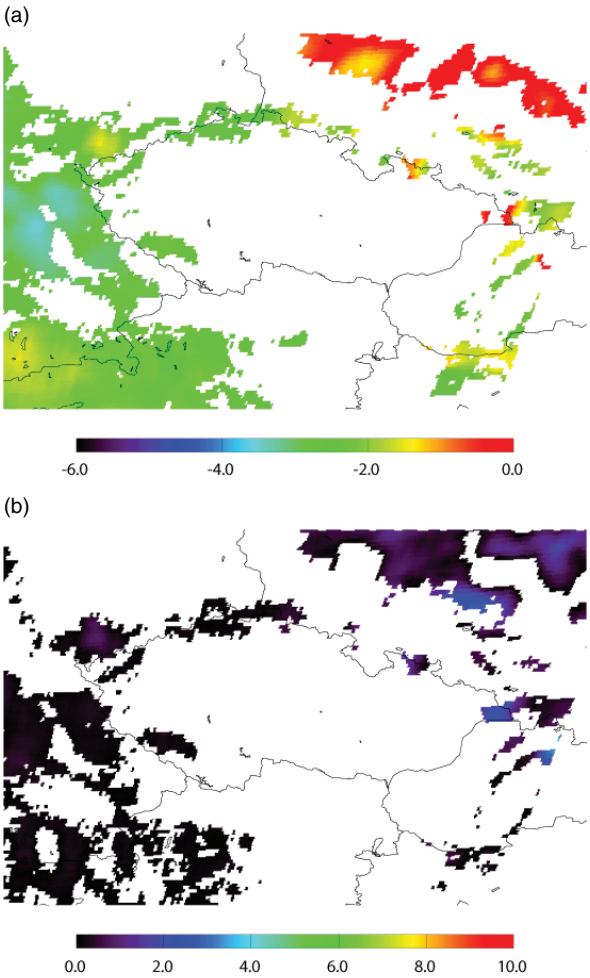

Figure 3. Images of 31 May 2008 nowcast time period 1100 UTC (a) 8.7–10.8 μm channel difference and (b) 8.7–10.8 μm 30 min trend.

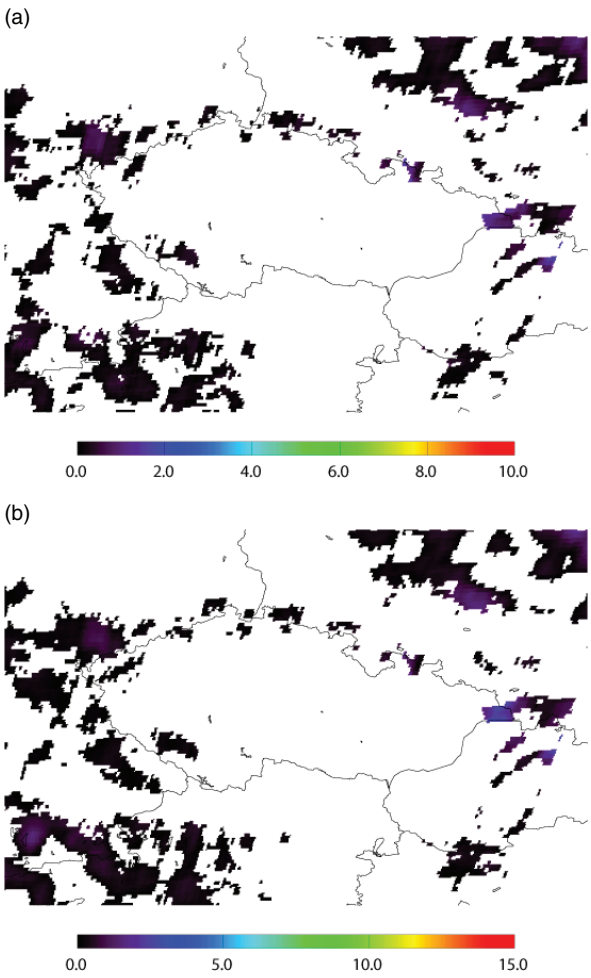

Figure 4. Images of 31 May 2008 nowcast time period 1100 UTC (a) 'tri-channel' 15 min trend and (b) tri-channel 30 min trend.

on IR brightness temperatures allows forecasters to gain insight into the environment upon which the CI nowcasts are being made. The forecaster can better determine regions where false nowcasts are being made and which regions should be given more attention. The Mecikalski and Bedka (2006) CI nowcast, shown in Figure 5(a), represents the method using only interest fields as would be available on the GOES-12 satellite. Here three regions along the northern border of the Czech Republic are seen where CI is being forecasted to occur. The Mecikalski and Bedka (2006) CI nowcast also produces nowcasts over southern Poland, where a layer of cirrus was located during this time period. These nowcasts, which were not associated with any convective growth in the future, can easily be ruled out by forecasters by examining the IR brightness temperature image, or overlaying the nowcasts on a visible image, which is also possible. Use of a convective cloud masking approach like that of Berendes *et al*. (2008) would assure that regions with cirrus overcast would not be considered. Cirrus clouds often cause substantial FARs in the Mecikalski and Bedka (2006) CI algorithm when thin cirrus clouds are present (Mecikalski *et al*., 2008).

Figure 5(b) shows the MSG CI nowcast for the same time period. In this instance the CI nowcasts for the Czech Republic border are nearly identical to those made using the Mecikalski and Bedka (2006) method. However, nowcasts in the region of cirrus over Poland have decreased significantly. Also, the MSG CI nowcast allows for the CI strength indicators, shown as purple and cyan pixels as described in Section 2.2, based on how many of the 19 interest fields were met. These indicators have yet to be studied in further detail regarding their physical basis.

Figures 6(a) and (b) shows the maximum radar reflectivity for 1100 UTC and 1130 UTC for the same area. At 1100 UTC only slight signals in reflectivity across most of the northern Czech Republic border (Figure 6(a)). Thirty minutes later, however, reflectivities exceeding 35 dBZ are seen. These locations (Figure 6(b)) at 1130 UTC correlate well to the regions where CI nowcast were made for both the Mecikalski and Bedka (2006) and MSG nowcasts. However, the northern-most cell along the border was not nowcast by either method, suggesting that this cell may be associated with strong orographic lifting effects, which can be difficult to detect *via* 15 min satellite data.

Copyright © 2010 Royal Meteorological Society

DOI: 10.1002/met

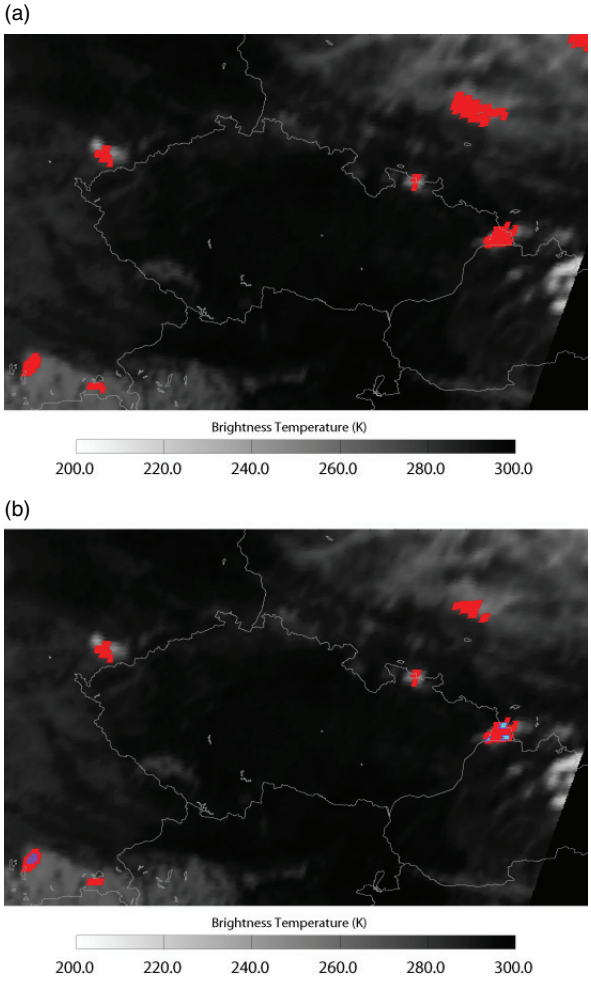

Figure 5. The CI nowcast product overlaid on 10.8 μm brightness temperatures for 31 May 2008 at 1100 UTC over the Czech Republic for the (a) Mecikalski and Bedka (2006) method and (b) using MSG specific interest fields.

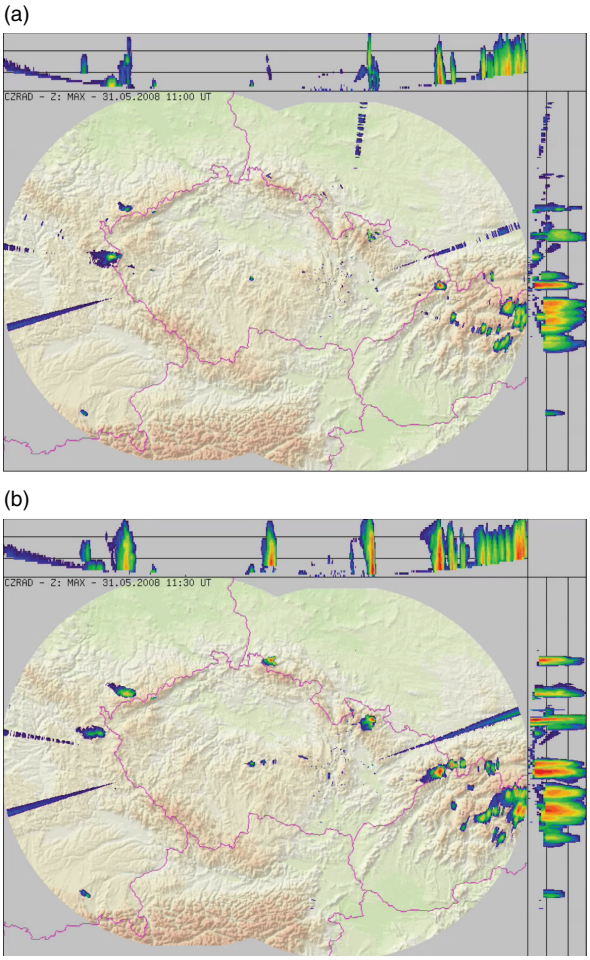

Figure 6. Maximum radar reflectivity for 31 May 2008 over the Czech Republic for (a) 1100 UTC and (b) 1130 UTC. Areas of yellow shading represent maximum reflectivity exceeding 35 dBZ. (Image courtesy of Martin Setvak).

As noted above, the nowcasts for both the Mecikalski and Bedka (2006) and MSG methods produced very similar nowcasts over the area of primary interest along the northern border Czech Republic. However, it was also noticed that the MSG CI nowcast did reduce false nowcasts over a region of cirrus with no convective interest. Upon reviewing the entire scene over central Europe, shown in Figures 7(a) and (b), this effect can be seen on a much larger scale. The Mecikalski and Bedka (2006) method (Figure 7(a)) produces many false nowcasts, particularly over Poland and France where cirrus clouds are present. Including the MSG specific interest fields, shown in Figure 7(b), significantly reduces these nowcasts over regions where no CI would be expected to occur during this time period.

3.2. 7 February 2008

The 7 February 2008 case study represents a typical convective summertime event over the southern portions of Africa. These events, which are very common during Southern Hemisphere summer due to highly unstable conditions, often contribute to dangerous flooding and other severe weather. The lack of radar coverage over most of Africa makes forecasting and tracking these events very difficult, with validation nearly impossible. However, since the MSG satellites continuously view this area, a satellite tool to predict and follow convection would prove to be very useful. Fortunately, radar data are readily available from the South African Weather Service over the majority of South Africa, which provides a good testing ground for satellite CI applications. Similar to the case discussed previously, two versions of the CI nowcast were produced and will briefly be discussed.

Figures 8 and 9 show the two CI nowcasts and the appropriate radar images respectively for the 1200 UTC CI nowcast time period. Similar to the 31 May 2008 case both CI nowcast methods produce similar results over areas of convective interest, with nowcasting lead times around 30 min. However, again it is seen that the MSG CI nowcast reduces nowcasted pixels over non-convective environments where cirrus or stratus may be present, seen in the northeastern-most corners of Figure 8. This reduction is due to the additional IR tests applied, and, in effect, convective clouds are the only cases in which $>12-15$ CI indicators can be achieved. Also, this

Copyright © 2010 Royal Meteorological Society

DOI: 10.1002/met

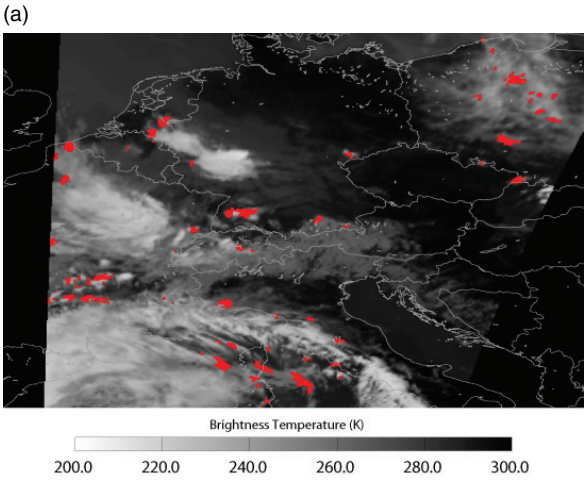

Figure 7. CI nowcast overlaid on 10.8 μm brightness temperatures for 31 May 2008 at 1100 UTC over central Europe from the (a) Mecikalski and Bedka (2006) method and (b) using MSG specific interest fields.

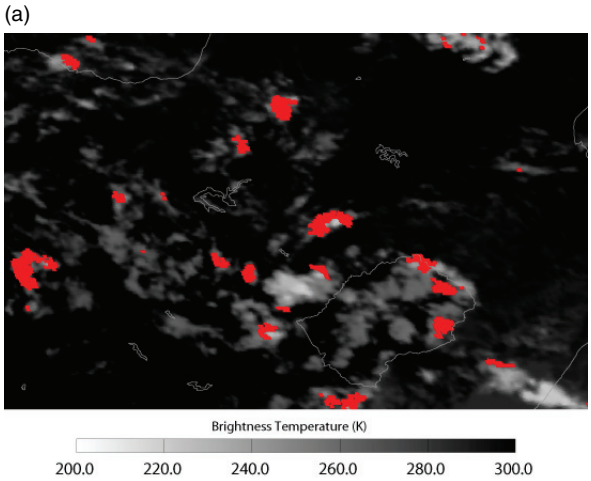

Figure 8. The CI nowcast product overlaid on 10.8 μm brightness temperatures for 7 February 2008 at 1030 UTC over South Africa for the (a) Mecikalski and Bedka (2006) method and (b) using MSG specific interest fields.

case provides a good look at the CI strength indicators provided by the addition of the GII instability fields (Figure 8(b)). Areas of 'strong' CI indicators, or where all 19 of the interest field thresholds were met and shown as cyan pixels, are bounded by red pixels, where only 16 of the 19 CI interest field threshold were met. This suggests that there may be some physical basis behind the CI strength indicators that should be studied further.

4. Discussion

From the analysis of 10 CI case studies over South Africa and central Europe, one of each of which were presented briefly above, a concept for which the integration of MSG specific interest fields into a CI nowcast has been shown to possibly provide additional information into the CI nowcasting process in which physical processes leading to development of convection from a satellite perspective may be better understood. From the 31 May 2008 case study example, it was shown that the new MSG specific interest fields do show skill in detecting regions of CI interest. This case study also showed that by adding these MSG specific interest fields, false CI alarms over regions where convection is not likely to occur were significantly reduced. The specific amount of this reduction is not known and should be quantified further over a much larger dataset to draw conclusions. However, visual analysis of the larger region during this and other cases used in this study suggests that it may easily be possible to reduce overall false alarms by 5% or more.

The 7 February 2008 case study showed an example of how these methods may be used over the African continent, where radar coverage is scarce. Again, it was shown that including the MSG specific interest fields did slightly reduce false alarms over the area of interest. The 7 February 2008 case study also provided a good example of the possibilities for further understanding of the physical processes of CI from the CI strength indicators. Techniques for implementing a CI 'severity' nowcasts should be tested further.

5. Conclusions

The prediction of CI on the 0–1 h time frame from a geostationary satellite prospective provides a valuable

Copyright © 2010 Royal Meteorological Society

DOI: 10.1002/met

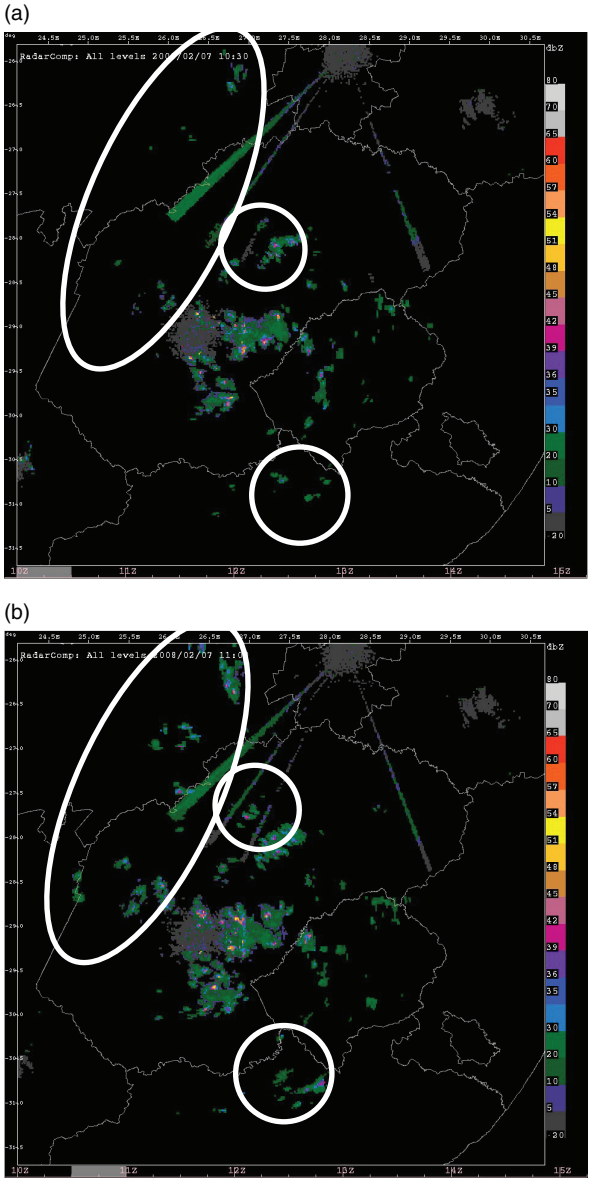

Figure 9. Maximum radar reflectivity for 7 February 2008 over South Africa for (a) 1030 UTC and (b) 1100 UTC. (Image courtesy of the South African Weather Service).

tool for operational forecasters to help protect both life and property, particularly over regions where radar data are limited or not available. A scoring based CI nowcasting product has been developed by Mecikalski and Bedka (2006) for use on the GOES system and this paper's goal was to assess the possible improvements that including MSG specific interest fields developed by Mecikalski *et al*. (2010) may provide. Through the analysis of 10 case studies over central Europe and South Africa it has been shown that by including MSG specific interest fields provides similar CI nowcasting ability to those provided by the proven Mecikalski and Bedka (2006) method over regions of convective interest. The inclusion of these MSG specific interest fields also showed a significant reduction in false CI alarms over the Mecikalski and Bedka (2006) method where convection would not likely occur, however, this exact amount is yet to be determined. The reduction in false alarms is likely caused by the fact that only convective clouds pass many tests for cloud depth, cloud-top glaciation, and updraft strength. It may also be possible to make more physical-based CI 'severity' nowcasts by including the additional interest fields. However, the physical basis and performance of these CI severity nowcasts must be studied in further detail.

An external study contract has been put in place to validate these findings over Europe using the techniques described in this paper. This follow-on study will include the use of radar, lightning and severe storm reports from the European Severe Storm Laboratory to validate convective initiation detection and identify signals conducive to the occurrence of severe weather and lightning. Also, it is expected that the ability to detect the onset of convective initiation and other weather phenomena by use of techniques based on satellite data are expected to greatly improve once the next generation of geostationary satellites (GOES-R and Meteosat Third Generation) is launched within the next decade.

Acknowledgements

The authors would like to thank Johannes Schmetz from EUMETSAT for providing support for this research. The authors would also like to thank Kristopher Bedka from the University of Wisconsin's Cooperative Institute for Meteorological Satellite Studies for providing assistance with the CI algorithm. The authors also thank Hans-Joachim Lutz and Phillip Watts from EUMETSAT for providing data processing for the cloud mask used in this study.

References

Ackerman S. 1996. Global satellite observations of negative brightness temperature differences between 11 and 6.7 μm. *Journal of the Atmospheric Sciences* **53**: 2803–2812.

Adler RF, Fenn DD. 1979. Thunderstorm intensity as determined from satellite data. *Journal of Applied Meteorology* **18**: 502–517.

Berendes TA, Mecikalski JR, Mackenzie WM Jr., Bedka, KM, Nair US. 2008. Convective cloud identification and classification in daytime satellite imagery using standard deviation limited adaptive clustering. *Journal of Geophysical Research* **113**: D20207, DOI:10.1029/2008JD010287.

Ellrod GP. 2004. Loss of the 12 μm "Split Window" band on GOES-M: impacts on volcanic ash detection. *Journal Volcanic Geothermal Research* **135**(1–2): 91–103.

Koenig M, de Coning E. 2009. The MSG global instability indices product and its use as a nowcasting tool. *Weather and Forecasting* **24**: 272–285.

Lutz HJ. 2007. Cloud detection for MSG – algorithm theoretical basis document, EUM/MET/REP/07/0132, 26 pp. Available at www.eumetsat.int. Accessed 2007.

Mackenzie WM Jr, Harris RT, Siewert CW, Mecikalski JR. 2010. Convective and lightning initiation estimation based on use of the GOES 3.9 micron channel. *Journal of Geophysical Research* (Submitted).

Mecikalski JR, Bedka KM. 2006. Forecasting convective initiation by monitoring the evolution of moving cumulus in daytime GOES imagery. *Monthly Weather Review* **134**: 49–78.

Mecikalski JR, Bedka KM, Paech SJ, Litten LA. 2008. A statistical evaluation of GOES cloud-top properties for nowcasting convective initiation. *Monthly Weather Review* **136**: 4899–4914.

Mecikalski JR, Feltz WF, Murray JJ, Johnson DB, Bedka KM, Bedka ST, Wimmers AJ, Pavolonis M, Berendes TA, Haggerty J,

Copyright © 2010 Royal Meteorological Society

Minnis P, Bernstein B, Williams E. 2007. Aviation applications for satellite-based observations of cloud properties, convection initiation, in-flight icing, turbulence, and volcanic ash. *Bulletin of the American Meteorological Society* **88**: 1589–1607.

Mecikalski JR, Mackenzie WM Jr, Bedka, KM. 2008. *Algorithm for Convective Initiation for GOES-R*. NOAA NESDIS Algorithm Theoretical Basis Document. 30pp.

Mecikalski JR, Mackenzie WM Jr, Koenig M, Muller SA. 2010. Cloud-top properties of growing cumulus prior to convective initiation as measured by Meteosat Second Generation. Part 1. Infrared fields. *Journal of Applied Meteorology and Climatology* (in press).

Nair U, Weger R, Kuo K, Welch R 1998. Clustering, randomness, and regularity in cloud fields 5. The nature of regular cumulus cloud fields. *Journal of Geophysical Research* **103**(D10): 11363–11380.

Prata AJ. 1989. Observations of volcanic ash clouds in the 10–12 μm window using AVHRR/2 data. *International Journal of Remote Sensing* **10**: 751–761.

Purdom JFW. 1976. Some uses of high-resolution GOES imagery in the mesoscale forecasting of convection and its behaviour. *Monthly Weather Review* **104**: 1474–1483.

Purdom JFW. 1982. Subjective interpretation of geostationary satellite data for nowcasting. In *Nowcasting*, Browning KA (ed.). Academic Press: St Louis, USA; 149–166.

Riehl H, Schleusener RA. 1962. On identification of hail bearing clouds from satellite photographs. Atmospheric Science Technical Paper, No. 27. Colorado State University: Fort Collins, Co; 7pp.

Roberts RD, Rutledge S. 2003. Nowcasting storm initiation and growth using GOES-8 and WSR-88D data. *Weather and Forecasting* **18**: 562–584.

Rosenfeld D, Woodley WL, Lerner A, Kelman G, Lindsey DT. 2008. Satellite detection of severe convective storms by their retrieved vertical profiles of cloud particle effective radius and thermodynamic phase. *Journal of Geophysical Research* **113**: D04208, DOI:10.1029/2007JD008600.

Schmetz J, Pili P, Tjemkes S, Just D, Kerkmann J, Rota S, Ratier A. 2002. An introduction to Meteosat Second Generation (MSG). *Bulletin of the American Meteorological Society* **83**: 977–992.

Schmetz J, Tjemkes SA, Gube M, van de Berg L. 1997. Monitoring deep convection and convective overshooting with METEOSAT. *Advances in Space Research* **19**: 433–441.

Schmit TJ, Gunshor MM, Menzel WP, Gurka JJ, Li J, Bachmeier AS. 2005. Introducing the next-generation Advanced Baseline Imager on GOES-R. *Bulletin of the American Meteorological Society* **86**: 1079–1096.

Setvak M, Doswell CA III 1991. The AVHRR Channel 3 cloud top reflectivity of convective storms. *Monthly Weather Review* **119**: 841–847.

Setvak M, Rabin RM, Doswell CA III, Levizzani V. 2003. Satellite observations of convective storm tops in the 1.6, 3.7 and 3.9 μm spectral bands. *Atmospheric Research* **67–68**: 607–627.

Strabala KI, Ackerman SA, Menzel WP. 1994. Cloud properties inferred from 8–12-μm data. *Journal of Applied Meteorology* **33**: 212–229.

Wulfmeyer V, Behrendt A, Bauer HS, Kottmeier C, Corsmeier U, Blyth A, Craig G, Schumann U, Hagen M, Crewell S, Di Girolamo P, Flamant C, Miller M, Montani A, Mobbs S, Richard E, Rotach WM, Arpagaus M, Russchenberg H, Schlüssel P, König M, Gärtner V, Steinacker R, Dorninger M, Turner DD, Weckwerth T, Hense A, Simmer C. 2008. RESEARCH CAMPAIGN: the convective and orographically induced precipitation study. *Bulletin of the American Meteorological Society* **89**: 1477–1486.

Copyright © 2010 Royal Meteorological Society